Extended study of crystallization kinetics for Se–Te glasses

Roman Svoboda · Jiří Málek

Abstract Crystallization kinetics of chosen compositions from Se–Te glassy system were studied under non-isothermal conditions depending on particle size using differential scanning calorimetry. The purpose of this article is to demonstrate the extent of information accessible by the modern kinetic analysis provided by the differential scanning calorimetry, and to suggest its importance and merit for the development of new, high-tech PCM materials. The crystallization kinetics was described in terms of the nucleation-growth Johnson–Mehl–Avrami model. Complexity of the crystallization process was in this case represented by very closely overlapping consecutive competing surface and bulk nucleation-growth mechanisms. Mutual interactions of both mechanisms as well as all other observed effects were explained in terms of thermal gradients, surface crystallization centers arising from the sample preparation treatments, and changing amount of volume nuclei originating from the combination of pre-nucleation period, and the very glass preparation phase. Accent was laid on the merits resulting from interpretations of characteristic kinetic functions. A new criterion for quick determination of the dominating crystallization mechanism—surface or bulk—was introduced.

Keywords Crystallization kinetics · DSC · JMA model · $Se_{(1-y)}Te_y$

R. Svoboda (✉) · J. Málek
Department of Physical Chemistry, Faculty of Chemical Technology, University of Pardubice, Studentska 573, 532 10 Pardubice, Czech Republic
e-mail: roman.svoboda@upce.cz

Introduction

Chalcogenide glasses belong to very important materials nowadays. It is their unique properties (e.g., low temperatures of glass transition and crystallization, large variety in crystallization tendency strongly depending on actual compositions, great distinction of amorphous and crystalline states by means of their reflectivity or electrical conductivity, numerous photoconductive effects or high transmittance in near, middle, and far infrared region, etc.) that make them irreplaceable for numerous hi-tech applications, such as sophisticated devices and elements for infrared optics and optoelectronics (fibers, planar guides, and lenses), various electronic thresholds and memory switches, or large capacity data-storage media (i.e., non-volatile PCRAMs or optically recorded CDs, DVDs, and BlueRay Discs). In all these applications, the crystallization process plays a vital role to either enable/represent the very technological mechanism or, on the contrary, to prevent the ideal glass from degradation. In this regard, the knowledge of detailed crystallization kinetics appears to be very important as it can provide the ability to predict the crystallization behavior in hypothetical, not yet prepared materials by revealing the basic mechanisms and general principles valid for particular structural units or their combinations. Confirmation of the above mentioned observations is found from the increasing numbers of crystallization kinetics studies in perspective chalcogenide systems (e.g., [1, 2]).

The crystallization kinetics has undergone a significant progress in the past, and the present day calculation methods have already become highly sophisticated [3]. Nevertheless, there is still a weak spot present in the calculations, namely in those regarding the analysis of multiple overlapping and mutually interacting processes. In the

case of interacting processes, the separation of the individual signals corresponding to particular phenomena may be significantly more complicated than it might appear. A simple subtraction of both signals (even if performed on the basis of one of the relevant theoretical models) may still bear large error because of not accounting for the influences of thermal gradients or mutual interactions of the involved processes. The actual quality of the results is therefore highly dependent on their critical evaluation. For this reason, the detailed and precise qualitative understanding to the kinetics of the particular involved mechanisms is of great importance in the case of complex crystallization processes. In this regard, it is the kinetic study performed depending on particle size that provides the largest portion of essential information.

One of the most common and widely spread instrumental techniques for studying the crystallization kinetics in solids is differential scanning calorimetry (DSC)—a device that registers and records the evolved and expended heat depending on applied temperature program. The kinetic equation of DSC curve can be described [4] as follows:

$$\Phi = \Delta H \cdot A \cdot e^{-E/RT} \cdot f(\alpha) \tag{1}$$

where Φ is the measured heat flow, ΔH is the crystallization enthalpy, A is the pre-exponential factor, E is the apparent activation energy of the process, R is the universal gas constant, T is temperature, and $f(\alpha)$ stands for an expression of a kinetic model with α being conversion. There is a large number of kinetic models; however, in case of crystallization in glasses, only very few are actually being applied. One of the most important models in this respect is the physically meaningful nucleation-growth Johnson–Mehl–Avrami model, JMA(m) [5–8]:

$$f(\alpha) = m(1 - \alpha)[-\ln(1 - \alpha)]^{1-(1/m)} \tag{2}$$

where m is the parameter reflecting nucleation and crystal growth mechanisms, as well as the crystal morphology. The equation (2) was derived strictly for isothermal conditions with additional assumptions as follows: the growth rate of a newly formed phase is controlled only by temperature and is independent of time and previous thermal history; nucleation is either homogeneous or heterogeneous on randomly distributed active centers; and growing crystals have low anisotropy. Nevertheless, it was shown by Henderson [9, 10] that the validity of this model can be extended also to non-isothermal conditions. This extension may be done under an assumption that the entire nucleation process takes place during early stages of the transformation and becomes negligible afterward during the very crystal growth.

In our study, a thorough kinetic analysis of chosen compositions from the glassy Se–Te system was performed to investigate the change in crystallization behavior with substitution of selenium matrix by tellurium atoms. This article is in fact a continuation and completion of our recent research on phase transformations in the Se–Te system [11–13], detailed crystallization kinetics study for $Se_{70}Te_{30}$ was already published [13]—the results for this material will thus be mentioned only briefly. The authors would like to further mention that, apart from the obvious practical importance of the crystallization kinetics results for Se–Te glasses, the crystallization behavior in the studied system is quite interesting and can also serve as a model example of complex combination of mutually interacting processes. Considering the former, the authors would like to introduce a new concept of interpretation of DSC data for complex physical processes.

Experimental

Glasses of chosen compositions ($Se_{90}Te_{10}$, $Se_{80}Te_{20}$, and $Se_{70}Te_{30}$) were prepared from pure elements (5 N, Sigma Aldrich) by the classical melt-quenching method. Adequate amounts of elements were accurately weighted into a fused silica ampoule, degassed, and sealed. The batched ampoule was annealed in the rocking furnace at 650 °C for 24 h. Glasses were then prepared from their melts by quenching the ampoules in water. The amorphous nature of each glass was checked by X-ray diffraction, and homogeneity of the glasses was verified from the position of the relaxation peak at T_g, which was measured under defined thermal history for samples taken randomly from the bulk glass.

Crystallization behavior of the prepared glasses was studied using a conventional DSC 822^e (Mettler, Toledo) equipped with cooling accessory. Dry nitrogen was used as the purge gas at a flow rate of 20 cm^3 min^{-1}. The calorimeter was calibrated through the use of melting temperatures of In, Zn, and Ga. Baseline was checked daily. Each prepared glass was ground to a set of powders with defined particle sizes: 20–50, 50–125, 125–180, 180–250, 250–300, and 300–500 μm. In addition, bulk samples were prepared by cracking a thin layer of as-prepared bulk glass (no other operations, such as sawing, grinding, or polishing were performed to minimize creation of artificial surface defects). In the case of powders, a thin layer of the material was spread on the bottom of aluminum pans to improve thermal contact; masses of the samples varied between 9 and 10 mg.

Concerning thermal histories, a specific temperature program needed to be applied because of a close vicinity of the glass transition and crystallization phenomena in the studied materials. For this reason, the sample had to be first brought to thermal and structural equilibrium by annealing at temperatures above T_g to minimize the relaxation effect during the consequent measurement. The temperature and

duration of annealing are needed to be chosen carefully because of the danger of possible starting of the crystallization process at too high temperature, which would, naturally, falsify any consecutive results. Therefore, these temperatures were intensively tested to verify zero allowance of the proceeding crystallization—cyclic relaxation experiments over T_g finishing at the tested annealing temperatures were applied for each studied material. In this way, the total time spent by the glassy sample at the annealing temperature exceeded 2 h, while no changes in the absolute magnitude of the relaxation effects at T_g or changes in the difference between heat capacities of undercooled liquid and glass (indicating formation of a partially crystalline material) were observed. The parameters of the isothermal step were thus optimized not only with regard to the crystallization process but also concerning the maximum stability and reproducibility of the measuring system (thermal gradients in the DSC cell, purge gas flow fluctuations, influence of surrounding experimental conditions, and their stability). The final temperature program then consisted of a short 5-min isotherm at the annealing temperature (60 °C for $Se_{90}Te_{10}$, and 70 °C for $Se_{80}Te_{20}$ and $Se_{70}Te_{30}$), subsequent cooling to 20 °C at -10 K min^{-1}, and final heating step to 180 °C performed at heating rates varying from 1 to 30 K min^{-1}. Under these conditions, no intervention of the glass transition effect into the crystallization processes was observed for the whole interval of applied heating rates. In addition, the annealing isotherm served also as a pre-nucleation period, at least roughly unifying number of bulk crystallization centers (with respect to their initial number driven only by the exact "position" of the particular piece of glass in the ampoule during the preparation of the glass and by the effective cooling rate resulting from this "position"). Each measurement was reproduced two times to estimate experimental errors.

The questions of proper data acquisition and origins of possible thermal gradients in DSC crucibles have already been in detail discussed in [13], to which the reader for further information is referred. All the rules were applied also in the case of the $Se_{90}Te_{10}$ and $Se_{80}Te_{20}$ materials studied within the framework of this article. It can be stated also for these two materials that, following the above suggested set of procedures, nearly perfect reproducibility was achieved not only for samples originating from the same batch of glass but also for the samples coming from separately (reproducibly) prepared glassy materials.

Results and discussion

This section will be divided into two parts. In the first part, results of the so-called primary kinetic analysis will be

introduced and discussed—determination of the activation energy and of the dominating crystallization mechanism belong in here. The second part will then include calculations (and their results) based on simple data transformations, i.e., evaluation of a suitable kinetic model and its parameters and interpretation of kinetic functions $y(\alpha)$ and $z(\alpha)$.

Primary kinetic analysis

As was already suggested in the introductory text to this section, the primary kinetic analysis will involve determination of apparent activation energy of crystallization and revelation of the basic crystallization mechanism for all the three studied chalcogenide glasses. The apparent activation energy E_A is a crucial parameter for all consequent kinetic calculations. Therefore, a number of methods was developed over time to maximize accuracy and reliability of E_A evaluation. Nevertheless, the two probably most commonly and often used are those by Kissinger [14] and Friedman [15]. The Kissinger method is applicable only under non-isothermal conditions and is based on the shift of the maximum of the crystallization peak T_p with heating rate q^+ according to the following equation:

$$\ln\left(\frac{T_p^2}{q^+}\right) = -\frac{E_A}{RT_p} + \text{const.} \tag{3}$$

This method is based on an assumption that the conversion degree α corresponding to the maximum crystallization rate is constant and independent of experimental conditions. This assumption, on the other hand, is in fact the fundamental essence of the Friedman's isoconversional method. In this method, the apparent activation energy is calculated for various degrees of conversion according to the following equation:

$$\ln(\Phi_\alpha) = -\frac{E_A}{RT_\alpha} + \text{const.} \tag{4}$$

where Φ_α and T_α are the specific heat flow and temperature corresponding to certain chosen value of conversion α, respectively. The experimental data are in this case obtained from crystallization curves measured at different heating rates and are plotted for each value of α separately. In this way, eventually the dependence of activation energy E_A on the degree of conversion α is obtained. Owing to the large influence of experimental conditions on the data quality of the crystallization peak tails, it is a common practice to consider only values of E_A obtained for the interval $\alpha = 0.3 - 0.7$ when calculating average value. In an ideal case of a single and simple crystallization process, the apparent activation energy should be independent of the degree of conversion α.

The results obtained by applying the two aforementioned methods to the experimental data for all the three studied chalcogenide glasses and all the prepared fractions are listed in the Table 1. Graphical representation of the Kissinger method results is then given in Fig. 1. The particle size fractions were distributed according to the average particle size; value of 1 mm was assigned to the bulk specimen. The Friedman method was omitted from the figure as both methods provide fairly similar values of E_A anyway. The only exception from this consistency were the bulk values. It has already been mentioned earlier that in the case of $Se_{70}Te_{30}$ bulk samples, an extremely fast and extensive evolution of heat took place, which owing to the large thermal gradients and resulting lags significantly deformed the crystallization peak at higher heating rates. The other two compositions, on the other hand, were not affected by this effect; however, another complication occurred—namely, the tendency for separation of the two involved crystallization mechanisms which in the case of $Se_{90}Te_{10}$ bulk specimens have already resulted in largely pronounced shoulders deforming the peak completely. Similar issue occurred of course also in the case of some other high-particle-size fractions but only for few
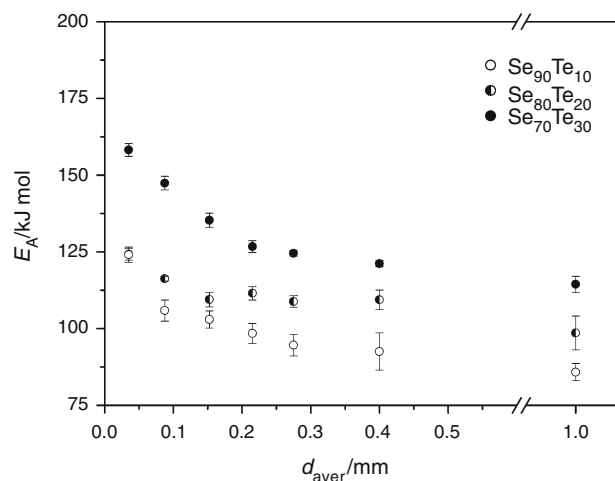

Fig. 1 Comparison of apparent activation energies determined for all three studied Se–Te glasses according to Kissinger depending on average particle size in particular fractions. Bulk samples were assigned $d_{aver} = 1$ mm

"extreme" heating rates, which were consequently excluded from the $E_{Friedman}$ determination. Main point of this discussion pointed at the Friedman method is then a

Table 1 Activation energies evaluated by Kissinger and Friedman methods, values of pre-exponential factor A obtained from curve-fitting and values of kinetic parameter m_{JMA} determined according to Málek and Šesták for all particle size fractions of the studied Se–Te glasses

Sample size/mm	$E_{Kissinger}$/kJ/mol	$E_{Friedman}$/kJ/mol	m_{Malek}	m_{Sestak}	ln (A/s)
$Se_{90}Te_{10}$					
0.020–0.050	124 ± 3	117 ± 6	1.2 ± 0.5	1.5 ± 0.3	34.7 ± 0.1
0.050–0.125	106 ± 4	106 ± 3	2.1 ± 0.4	2.4 ± 0.5	28.1 ± 0.1
0.125–0.180	103 ± 3	107 ± 2	2.0 ± 0.2	2.6 ± 0.6	26.9 ± 0.1
0.180–0.250	98 ± 3	92 ± 4	1.7 ± 0.3	2.5 ± 0.7	25.2 ± 0.2
0.250–0.300	95 ± 4	70 ± 5	1.4 ± 0.1	1.7 ± 0.3	24.0 ± 0.2
0.300–0.500	93 ± 6	95 ± 4	1.3 ± 0.1	1.5 ± 0.2	23.4 ± 0.8
Bulk	86 ± 3	–	7 ± 13	2.8 ± 0.3	23.0 ± 0.4
$Se_{80}Te_{20}$					
0.020–0.050	124 ± 2	123 ± 2	1.4 ± 0.1	1.7 ± 0.2	33.5 ± 0.1
0.050–0.125	116 ± 1	117 ± 1	1.3 ± 0.1	1.5 ± 0.1	30.2 ± 0.1
0.125–0.180	109 ± 2	115 ± 3	1.3 ± 0.1	1.6 ± 0.2	27.7 ± 0.2
0.180–0.250	112 ± 2	109 ± 3	1.2 ± 0.1	1.5 ± 0.1	27.9 ± 0.1
0.250–0.300	109 ± 2	104 ± 4	1.2 ± 0.1	1.5 ± 0.1	27.0 ± 0.1
0.300–0.500	109 ± 3	101 ± 3	3.6 ± 1.1	1.7 ± 0.2	26.9 ± 0.2
Bulk	99 ± 6	112 ± 4	12 ± 10	3.6 ± 0.9	23.4 ± 0.2
$Se_{70}Te_{30}$					
0.020–0.050	158 ± 2	150 ± 3	1.1 ± 0.1	1.3 ± 0.1	45.5 ± 1.2
0.050–0.125	147 ± 2	141 ± 5	1.1 ± 0.1	1.3 ± 0.1	41.4 ± 1.1
0.125–0.180	135 ± 2	128 ± 6	1.4 ± 0.5	1.4 ± 0.1	37.8 ± 0.8
0.180–0.250	127 ± 2	120 ± 5	3.0 ± 1.5	1.5 ± 0.2	34.7 ± 1.1
0.250–0.300	125 ± 1	117 ± 5	5.4 ± 4.1	1.6 ± 0.1	32.5 ± 0.1
0.300–0.500	121 ± 1	113 ± 3	7.8 ± 4.8	1.5 ± 0.1	31.5 ± 0.1
Bulk	114 ± 3	148 ± 8	4.4 ± 3.2	5.1 ± 0.8	30.3 ± 0.4

suggestion not to overrate its evaluation potential. One should always bear in mind that if applied blindly, the isoconversional methods may in certain cases provide biased and unrealistic results because of the natural dependence of these methods on evaluation of α based solely on mathematical computation. Unlike the Kissinger method, where the determination of E_A is given by the actual physical essence of the crystallization process (maximum of the heat evolution rate is driven entirely by the fundamental crystallization mechanism), which in addition is almost independent of the experimental conditions, the evaluation according to the Friedman method is heavily dependent on the actual shape of the peak and baseline approximation method (due to the purely mathematical calculation of α) and therefore, correspondingly, the results of this method may be largely influenced by every possible change in experimental conditions that can occur either with the change of heating rate or simply with the long-term duration of the experiments sequence.

Nevertheless, if we look back at the Fig. 1, several conclusions can be drawn. It can be seen that the activation energy of the crystallization process E_A increases with rising tellurium content. This is in perfect agreement with what is known about selenium and tellurium molecular structures [16, 17], namely that the inter-chain distances are in the case of tellurium significantly shorter than those in selenium, and that delocalized bonds causing quasi-metallic conductivity are formed between the tellurium chains. In consequence, these bonds are most probably the reason for the crystallization activation energy increasing with higher tellurium content. In addition, the inter-chain bonding causes the material to react more homogeneously, which may be the corroborative argument for the faster tellurium-responsible internal crystallization (as will be shown later). Second conclusion derived from what is apparent in Fig. 1 is related to the very particle size dependencies of E_A. It can be seen that for all three studied glasses the apparent activation energy at first steeply decreases with increased glass grain size and then sort of limits toward the value assigned to bulk sample. This is in a perfect agreement with the fact that two crystallization mechanisms (surface and bulk) are involved in the overall process, where the surface crystallization has considerably higher activation energy. As the ratio of the involvement of the two mechanisms changes (due to decreasing number of surface defects and increasing "amount" of bulk material potentially containing/available for creation of volume nuclei), the averaged activation energy also follows monotonous convergent trend. The important term in previous sentence is the word "averaged," which is closely associated with the actual nature of inter-coupling between the two mechanisms.

Second block of thoughts and comments in this sub-section will be aimed at question of determination of the prevailing/dominant crystallization mechanism. A very thorough article on this topic was published by Ray and Day [18], who established several basic criteria (Φ_p—heat flow corresponding to the maximum of the peak, i.e., maximum peak height; and ΔT_{hh}—half-width of the peak, i.e., the width of the peak in the half of its height) and from the course of their dependence when plotted against the average particle size, they determined that the dominant crystallization mechanism is associated with surface defects and dislocations rather than with bulk nuclei. Although the criteria introduced by Ray and Day are very simple and relatively easy to evaluate, we would like to introduce in this article a new (to the authors' knowledge original) criterion that is also extremely simple to apply, but, in addition, it is independent of the most negative influences of experimental conditions (like those of e.g., thermal gradients arising from the arrangement of the DSC cell itself or gradients associated with the unideal thermal contact of particular sample grains with the bottom of DSC crucible) because of the only monitored quantity being T_p, which (as already discussed earlier) from the considered point of view is a very robust value to determine. This method is in fact based on the very essence of the idea of joint influence of bulk and surface crystallization mechanisms. The influence of the prevailing mechanism obviously determines/drives the crystallization process and takes control over its already moderate amounts of either surface defects and dislocations (in the case of surface crystallization) or bulk nuclei (in the case of volume crystallization). On the other hand, correspondingly, the number of preferred crystallization centers has to be very small for the secondary crystallization mechanism to dominate.

Implication of this fact can be well demonstrated with the help of Fig. 2, where the Kissinger plots for the three studied glasses are compared. It is well apparent that in the case of $Se_{70}Te_{30}$ the dependencies sort of "limit" to the one mostly influenced by the driving mechanism—volume/bulk crystallization is dominant in this glass. Similar but not very pronounced limitation is also apparent in the case of the $Se_{80}Te_{20}$ glass, where the bulk crystallization is also still present in a large extent. On the other hand, the plot for the $Se_{90}Te_{10}$ glass, where the intensities of surface and bulk crystallization mechanisms are comparable, does not show any limitation whatsoever. In order to quantify this phenomenon, it is suitable to plot the value of the temperature corresponding to the maximum of the crystallization peak T_p depending on the logarithm of the average particle size present in the respective fraction $\ln(d_{aver})$—see the right column in Fig. 2. In this depiction, the dependence limits toward either bulk or fine powder values according to the dominant crystallization mechanism. Conclusions resulting from this way of depiction are more definite and clear in

Fig. 2 *Left column* comparison of Kissinger plots for a set of particle size fractions measured for the three studied Se–Te chalcogenide glasses. *Right column* normalized crystallization mechanism plots introduced in this study to determine the dominating crystallization mechanism. See text for details
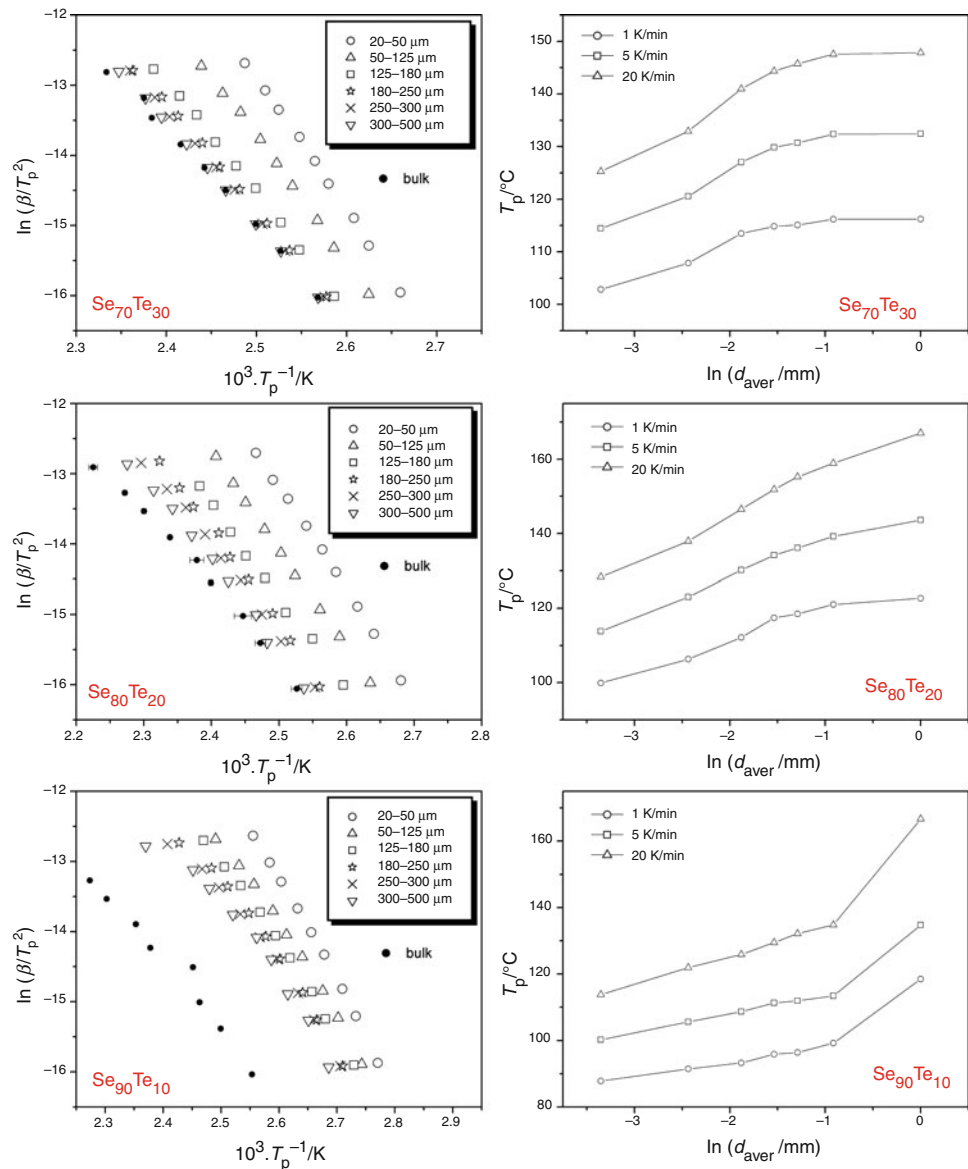

comparison with the left-side Kissinger-plot-type of evaluation. In the case of $Se_{70}Te_{30}$ glass, the dependence unambiguously limits to the bulk value, thus volume crystallization mechanism clearly dominates; for $Se_{80}Te_{20}$ glass, where surface crystallization manifests to a larger extent, no prevailing limitation is apparent because of both mechanisms being considerably overlaid in case of all particle size fractions and heating rates; and finally for the $Se_{90}Te_{10}$ glass with the surface crystallization starting to dominate, the dependence is all but limiting toward bulk value. The dependence for the $Se_{90}Te_{10}$ glass cannot be, however, described as limiting to the fine powders values (indicating fully dominant surface crystallization as does similar dependence in the case of e.g., $Ge_2Sb_2Se_5$ glass [19]), which has to be interpreted in terms of both the mechanisms still competing and manifesting themselves at

comparable levels. All the above mentioned conclusions derived on the basis of the newly introduced method were confirmed by applying the criteria developed by Ray and Day [18], which gave similar, yet not so straightaway, outcomes.

Secondary kinetic analysis

Apart from determination of apparent activation energy of crystallization, the second crucial step in kinetic analysis is the suggestion of an appropriate kinetic model [20]. For this reason, Málek [21, 22] introduced an algorithm based on the shape of characteristic functions $z(\alpha)$ and $y(\alpha)$. These functions are obtained by a simple transformation of experimental data; for non-isothermal conditions the characteristic functions are defined as

Fig. 3 Algorithm for determination of appropriate kinetic model based on values of maxima of $y(\alpha)$ and $z(\alpha)$ functions
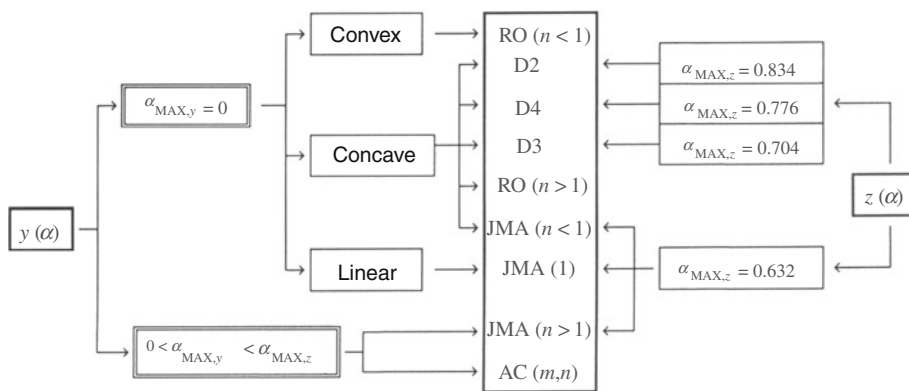
$$y(\alpha) = \Phi \cdot e^{E/RT} \tag{5}$$

$$z(\alpha) = \Phi \cdot T^2 \tag{6}$$

The introduced functions are in fact a universal way for determination of an appropriate kinetic model applicable to any kind of physical process. Determination of the most suitable kinetic model then utilizes both values of α, corresponding to the maxima of the characteristic functions ($\alpha_{max,y}$ and $\alpha_{max,z}$) and the overall shape of the functions. Based on this information, the optimal kinetic model can be chosen according to the algorithm [22] shown in Fig. 3 (where values calculated for several most common kinetic models are shown as well). However, the characteristic kinetic functions contain and can provide a lot more additional information when studied depending on particle size and composition. This will be demonstrated in the following text; akin interpretations can be made for $Se_{70}Te_{30}$ and $Ge_2Sb_2Se_5$ found in [13] and [19], respectively.

The first material to be discussed will be the $Se_{80}Te_{20}$ glass. In Fig. 4, characteristic functions for several chosen $Se_{80}Te_{20}$ particle size fractions are shown—each row corresponds to one particular fraction. Full set (with respect to particle size) of $z(\alpha)$ and $y(\alpha)$ functions for this material can be found in Online Appendix 1. It can be seen that the $z(\alpha)$ functions are perfectly consistent with respect to the applied heating rate confirming the uniform and invariable character of the crystallization process. In addition, the values of $\alpha_{max,z}$ generally point to the JMA model (theoretical value for this model is 0.632, see algorithm in Fig. 3). One could observe that in the case of coarser fractions, the values of $\alpha_{max,z}$ are slightly higher than what theory predicts. Nevertheless, as already shown in the case of $Se_{70}Te_{30}$ glass [13], the crystallization in Se–Te system is composed of two, to a certain level independent, processes—surface and bulk crystallization. As will be shown later, in the case of coarse $Se_{80}Te_{20}$ fractions, the bulk crystallization mechanism starts to manifest and the two processes tend to separate. This in consequence widens the total timescale/temperature interval during which the heat evolves, which owing to the preceding "secondary/minor"

process results in a shift of the main crystallization peak (and thus $\alpha_{max,z}$) toward higher conversion rates. In conclusion, both the shape and characteristics of the $z(\alpha)$ functions suggest and confirm the applicability of the JMA model.

If we look at the course of the $y(\alpha)$ functions, it is apparent that for the 20–50 and 50–125 μm fractions the $\alpha_{max,y}$ still unambiguously corresponds to the surface crystallization mechanism (approximate value of the JMA kinetic exponent $m_{JMA} = 1.3$). In addition, the shape of the functions is almost invariant with respect to applied heating rate. Nonetheless, with increasing coarseness, the bulk crystallization mechanism starts to manifest. In case of the 125–180-μm fraction, a very small shoulder could already be observed on the high-α side of the function, with increasing particle size then, naturally, the ratio between the manifestations of the two processes changes in favor of the bulk mechanism. The volume crystallization then becomes fully pronounced in the case of the bulk samples, where the shape of the $y(\alpha)$ function corresponds perfectly to a bulk crystallization mechanism with practically no trace of the surface onset. This is perfectly consistent with the idea of both crystallization mechanisms (surface and bulk) being present, where the intensity/representation of each particular process is given by the ratio of the number of surface defects to volume nuclei. That is, for the finest fractions—where during the grinding procedure, a large number of surface defects acting like crystallization centers were created and, moreover, the actual surface area was significantly increased—the prevailing mechanism is the surface crystallization. On the other hand, in the case of coarse fractions, the grinding was not so intensive (not applied at all in the case of bulk), the result of which was low amount of surface defects and a much more favorable ratio of the bulk/surface crystallization centers for the crystallization mechanism to be driven by the volume nucleation and continuing crystal growth.

The second trend apparent in Fig. 4 and Online Appendix 1 is a relatively strong dependence of the shape

Fig. 4 Normalized $y(\alpha)$ and $z(\alpha)$ functions corresponding to non-isothermal measurements of chosen particle size fractions of $Se_{80}Te_{20}$ glass. Particular *rows* match the individual studied fractions
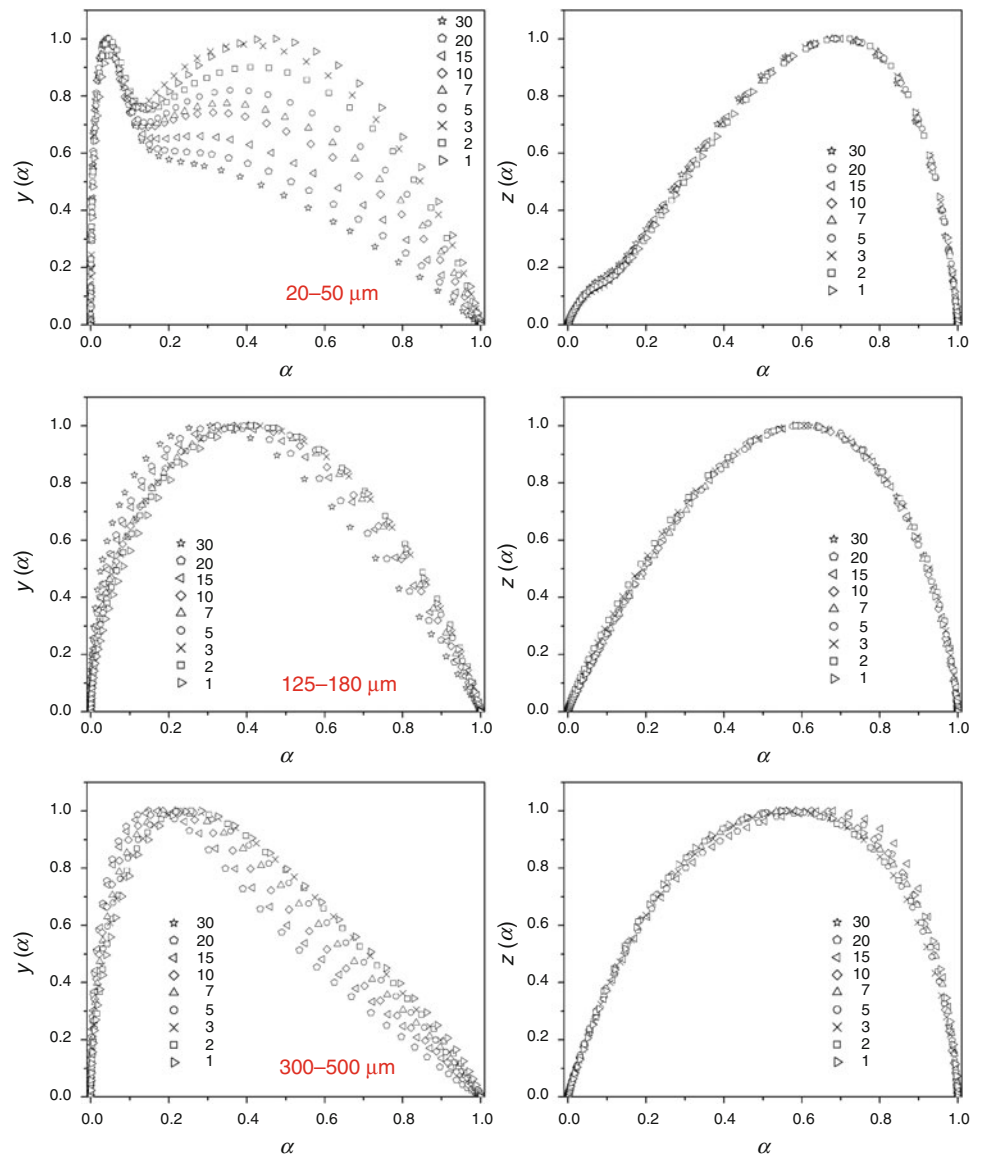
of $y(\alpha)$ functions on the heating rate in the case of fractions with comparable intensity of both involved processes. The bulk mechanism is here more pronounced at lower heating rates, while the surface crystallization manifests dominantly at higher heating rates. In order to explain this phenomenon, the concept of differing activation energies has to be employed. It is clearly apparent from the Fig. 1 and Table 1 that the surface crystallization appears to have slightly but still significantly higher activation energy than the bulk process. On the other hand, the three-dimensional kinetics is axiomatically slower and can be further decelerated by e.g., steric reasons. As can be seen from Fig. 4, the first process that takes place is always the surface crystallization that corresponds to the earliest heat evolution. Therefore, during the fast heating, the starting primary surface crystallization mechanism takes control over the

larger partition of the complex crystallization process (with more than enough energy being provided by the faster heating and thermal gradients causing the whole process to be allocated to higher temperatures), while the slower bulk mechanism does not have enough time to fully develop (in accordance with the concept of competing processes). Correspondingly, at low heating rates, it is the difference in activation energies that determines the outcome—although it is still the surface crystallization that starts the complex crystallization, the energy input (caused by the factual temperature increase plus heat evolved during the crystallization) is relatively low and an actual competition based on the difference in energy barriers (represented by the apparent activation energy E_A) takes place causing the bulk process to be more pronounced while "consuming" larger part of the provided energy.

If we compare the course of $y(\alpha)$ functions for the $Se_{70}Te_{30}$ [13] and $Se_{80}Te_{20}$ glasses, several differences are apparent. While in the case of the $Se_{70}Te_{30}$ glass, the transition between the two involved mechanisms is quite distinct, in the case of the $Se_{80}Te_{20}$ glass, their manifestation is kind of merged together. This is well consistent with the fact that for the $Se_{80}Te_{20}$ glass, the activation energies of the two mechanisms are relatively close (opposed to the $Se_{70}Te_{30}$ glass), which apparently results in the shift along the conversion rate axis. Moreover, it can be said that in the case of $Se_{80}Te_{20}$ glass, the surface crystallization mechanism becomes a lot more prominent, which is again consistent with results presented in former paragraphs.

Most conclusions derived for the $Se_{80}Te_{20}$ glass are valid also in the case of the $Se_{90}Te_{10}$ glass. The characteristic functions for chosen particle size fractions are for this material displayed in Fig. 5; full set is again shown in online Appendix 1. High consistency of the $z(\alpha)$ functions course with respect to experimental conditions and calculated values of $\alpha_{max,z}$ again confirm excellent applicability for the JMA model. When looking at the $y(\alpha)$ functions, it can also be said that in the case of the $Se_{90}Te_{10}$ glass, the surface crystallization mechanism is well pronounced and in fact seems to become the dominant one. Nevertheless, the bulk mechanism still remains present—in the case of bulk sample (see Online Appendix 1) the $y(\alpha)$ functions start to show strong dependence on heating rate similar to that displayed for the 300–500 μm fraction of $Se_{80}Te_{20}$ glass. This shift toward larger particle sizes again implicates larger portion of the surface crystallization mechanism involved. However, this is also the most

Fig. 5 Normalized $y(\alpha)$ and $z(\alpha)$ functions corresponding to non-isothermal measurements of chosen particle size fractions of $Se_{90}Te_{10}$ glass. Particular *rows* match the individual studied fractions
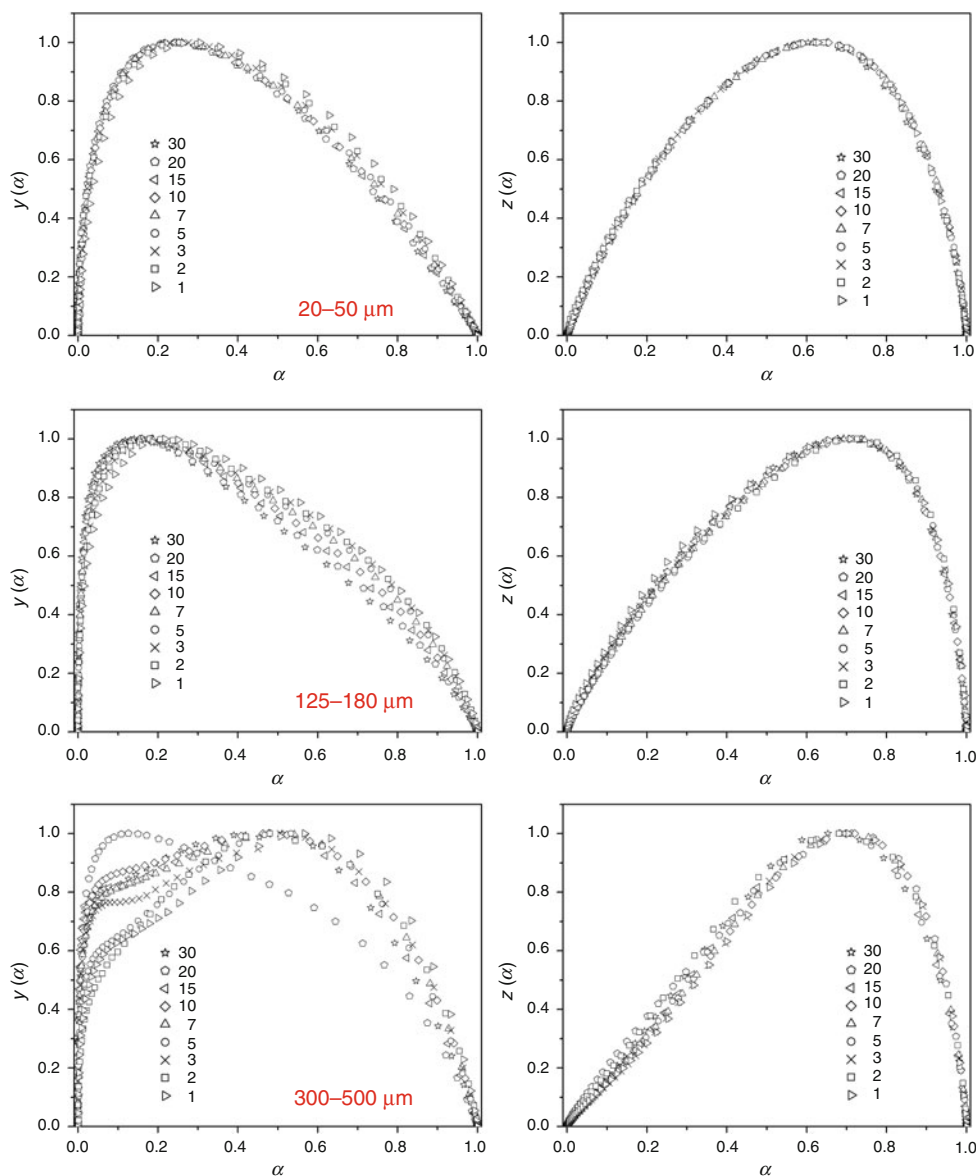
probable cause of the tendency for time-axis-based separation of the two processes occurring in the extreme cases of the surface-to-bulk nuclei number ratio (the 20–50-μm and bulk fractions). This is well apparent on the course of the $z(\alpha)$ function where in such case a shoulder appears. All these observations again well correspond to the detailed interpretations discussed above in the case of the $Se_{80}Te_{20}$ glass.

The actual results of the kinetic analysis for the three studied compositions from Se–Te glassy system studied within the framework of this publication are given in Table 1. The values of pre-exponential factor as well as the values of the kinetic parameter m_{JMA} were calculated as a mean value from all heating rates applied to the respective particle size fraction. The indexing in the case of the JMA model parameter corresponds to the method of evaluation—the index "Malek" denotes determination in accordance with Eq. 7 [23], which is based on the determination of the $\alpha_{max,y}$ value:

$$m = \frac{1}{1 + \ln(1 - \alpha_{max,y})} \qquad (7)$$

The index "Sestak" is then associated with evaluations according to the so called double-logarithm function—Eq. 8 [4]:

$$\frac{d\ln[-\ln(1 - \alpha)]}{d(1/T)} = -\frac{m \cdot E}{R} \qquad (8)$$

The linear dependence of the latter expression is also often considered a satisfactory condition for applicability of JMA model. Nevertheless, it is not recommended to use this method solely for this purpose [24].

It can be said that, while in the case of fine- and middle-sized particle size fractions, it is the evaluation according to Málek (Eq. 7) which provides more reasonable values (corresponding to what can be derived from the overall course in the shape of characteristic kinetic functions), in the case of coarse fractions and bulk, this method provides incorrect results because of the shift of the $\alpha_{max,y}$ toward too high values (caused by the partial separation of the two involved crystallization mechanisms). In the case of these samples, it is the double-logarithm function (Eq. 8) which provides correct results (or at least their reasonable estimates). It has to be, however, remarked that the double-logarithm function usually in these cases is not linear in the whole interval, and only the part corresponding to the dominant crystallization mechanism has to be chosen to obtain correct results. To conclude, as seen from the values of JMA kinetic parameter listed in Table 1, even in the case of relatively simple processes that can be (despite their mutual interaction) described by the physically meaningful JMA model, the very interpretation of the value of the kinetic parameter m_{JMA} depending on particle size may be difficult and misleading due to the complexity of the overall crystallization process or influence of thermal gradients not being taken into account during evaluations by Eqs. 7 and 8. In this regard, the authors recommend direct interpretation of the characteristic kinetic functions $z(\alpha)$ and $y(\alpha)$ rather than "blind" application of the above mentioned equations to obtain detailed and correct information about the complex crystallization processes.

Conclusions

Crystallization kinetics in $Se_{(1-y)}Te_y$ (for $y = 0.1$, 0.2 and 0.3) glassy system measured under non-isothermal conditions was described depending on particle size. The description was done in terms of the physically meaningful nucleation-growth JMA model. Apparent activation energy of the crystallization process for all the studied fractions was determined by the Kissinger and Friedman methods. The increase of activation energy with rising Te content can be attributed to the change of inter-chain distances in the glass. A new criterion for quick determination of the dominating crystallization mechanism—surface or bulk—was introduced. Complexity of the competing surface and bulk mechanisms for all three studied compositions was explained both, qualitatively and quantitatively. The obtained DSC data allowed explaining of the mutual interaction of the processes as well as of the origin of their sequentiality. Discussion over the observed effects, shifts in temperature, and deviations from ideal model behavior was conducted on the basis of thermal gradients, surface crystallization centers arising from the sample preparation treatments, and the amount of volume nuclei originating from the combination of pre-nucleation period and the very glass preparation phase. It can also be concluded that for materials with complex crystallization behavior, it is the direct interpretation of the characteristic kinetic functions that provides most important and most reliable information about the structural changes and involved physical mechanisms.

References

1. Patial BS, Thakur N, Tripathi SK. Crystallization study of Sn additive Se–Te chalcogenide alloys. J Therm Anal Cal. 2011;106:845–52.

2. Kotkata MF, Mansour ShA. Crystallization process analysis for $Se_{0.95}In_{0.05}$ and $Se_{0.90}In_{0.10}$ chalcogenide glasses using the contemporary isoconversional models. J Therm Anal Cal. 2011; 103:957–65.

3. Perejón A, Sánchéz-Jiménez PE, Criado JM, Pérez-Maqueda LA. Kinetic analysis of complex solid-state reactions. A new deconvolution procedure. J Phys Chem B. 2011;115:1780–91.

4. Šesták J. Thermophysical properties of solids, their measurements and theoretical analysis. Amsterdam: Elsevier; 1984.

5. Johnson WA, Mehl KF. Reaction kinetics in processes of nucleation and growth. Trans Am Inst Min Metall Pet Eng. 1939; 135:416–42.

6. Avrami M. Kinetics of phase change I—general theory. J Chem Phys. 1939;7:1103–12.

7. Avrami M. Kinetics of phase change. II—transformation-time relations for random distribution of nuclei. J Chem Phys. 1940;7: 212–24.

8. Avrami M. Granulation, phase change, and microstructure—Kinetics of phase change III. J Chem Phys. 1941;7:177–84.

9. Henderson DW. Experimental analysis of non-isothermal transformations involving nucleation and growth. J Therm Anal Calorim. 1979;15:325–31.

10. Henderson DW. Thermal analysis of non-isothermal crystallization kinetics in glass-forming liquids. J Non Cryst Solids. 1979;30:301–15.

11. Svoboda R, Krbal M, Málek J. Crystallization kinetics in Se–Te glassy system. J Non Cryst Solids. 2011;357:3123–9.

12. Svoboda R, Honcová P, Málek J. Enthalpic structural relaxation in Te–Se glassy system. J Non Cryst Solids. 2011;357:2163–9.

13. Svoboda R, Málek J. Interpretation of crystallization kinetics results provided by DSC. Thermochim Acta. 2011;526:237–51.

14. Kissinger HE. Reaction kinetics in differential thermal analysis. Anal Chem. 1957;29:1702–6.

15. Friedman HL. Kinetics of thermal degradation of char-forming plastics from thermogravimetry. Application to a phenolic plastic. New York: Wiley; 1964.

16. Bureau B, Danto S, Ma HL, Boussard-Plédel C, Zhang XH, Lucas J. Tellurium based glasses: a ruthless glass to crystal competition. Solid State Sci. 2008;10:427–33.

17. Bureau B, Boussard-Plédel C, Lucas P, Zhang X, Lucas J. Forming glasses from Se and Te. Molecules. 2009;14:4337–50.

18. Ray CS, Day DE. Identifying internal and surface crystallization by differential thermal analysis for the glass-to-crystal transformations. Thermochim Acta. 1996;280(281):163–74.

19. Svoboda R, Málek J. Particle size influence on crystallization behavior of $Ge_2Sb_2Se_5$ glass. J Non Cryst Solids. 2011;358: 276–84.

20. Málek J, Criado JM. Empirical kinetic models in thermal analysis. Thermochim Acta. 1992;203:25–30.

21. Málek J. Kinetic analysis of crystallization processes in amorphous materials. Thermochim Acta. 2000;355:239–53.

22. Málek J. The kinetic analysis of non-isothermal data. Thermochim Acta. 1992;200:257–69.

23. Málek J. A computer program for kinetic analysis of non-isothermal thermoanalytical data. Thermochim Acta. 1989;138: 337–46.

24. Málek J, Mitsuhashi T. Testing method for the Johnson–Mehl–Avrami equation in kinetic analysis of crystallization processes. J Am Ceram Soc. 2000;83:2103–5.